Applied Physics A (2025) 131:149
https://doi.org/10.1007/s00339-025-08254-y

Applied Physics A
Materials Science & Processing

Porosity effect on the thermal conductivity of sintered powder materials

J. M. Montes[1] · **F. G. Cuevas**[2] · **J. Cintas**[1] · **F. Ternero**[1]

Received: 5 November 2024 / Accepted: 8 January 2025

Abstract
In this work, the effective thermal conductivity of sintered powder materials is studied. The extensive literature related to the proposed models about this property in all kind of porous materials is reviewed, and a new equation is proposed as a function of the fully dense material conductivity, the porosity of the material and the tap porosity of the starting powder. This equation covers the porosity range of powder aggregates from the tap porosity to zero porosity, and also applies to sintered powders. The proposed equation has been experimentally validated by fitting to experimental data of metallic sintered powder materials measured at room temperature, resulting very good agreements. Also, alternative models proposed by other authors have been fitted to the same experimental data to check the relative goodness of the proposed model. The results allow to conclude that a percolation model can describe the behaviour of the effective thermal conductivity of sintered powder materials with low and medium porosity levels.

Keywords Thermal conductivity · Powdered materials · Granular materials · Sintered compacts · Foam materials · Modelling

1 Introduction

A porous material can be defined as a two-phase material consisting of a first phase that provides integrity to the whole (matrix) and envelops a second phase, which is the porosity. The porosity range can be very different: from small isolated pores, passing through interconnected porosity forming paths inside the matrix [1], to the extreme case of foamed materials [2], in which the matrix can be the minority phase of the system. The matrix, based either on polymers [3, 4], ceramics [5, 6] or metals [1], is in most cases constituted by a material clearly continuous, but also aggregates of different weakly bound particles, in a step previous to its final consolidation, can constitute the matrix. Thus, as described in [7], porous materials can be classified in three groups: packed beds where the particles contacts are points, consolidated solids with small contacts between particles, and porous solids with extensive contacts between particles. Other classifications of porous materials can also be found in the literature, for instance based on numerical criterions (low-porosity materials with porosities up to 10%, medium-porosity in the range 15%–85%, and high-porosity with values higher than 90%) [8], or on heat conduction mechanism criterions (isotropic porous materials with 'internal porosity', as sponges and foams, and those other with 'external porosity', constituted by grains and particulates) [9].

The study of the effective properties of porous materials, i.e., considering the effect of the porosity, is of great interest for a wide range of engineering applications, mainly including mechanical [1], thermal [10], electrical [11] and magnetic [12] properties. This work focuses on the thermal properties of porous materials.

Sometimes, the study of these effective properties is necessary in the finished product. Thus, the thermal properties of packed beds for catalyst or fuel cells electrodes [13], or foams in applications in which heat has to be transferred to a fluid moving inside the porous structure are of great interest. For instance, porous volumetric solar receivers made with

✉ J. M. Montes
jmontes@us.es

[1] Department of Engineering and Materials Science, Escuela Técnica Superior de Ingeniería, Universidad de Sevilla, Camino de los Descubrimientos, s/n, 41092 Sevilla, Spain

[2] Department of Chemical Engineering, Physical Chemistry and Materials Science, Escuela Técnica Superior de Ingeniería, Universidad de Huelva, Campus El Carmen, Avda. Tres de marzo s/n, 21071 Huelva, Spain

Published online: 30 January 2025

foamed materials are key components of concentrating solar power plants. They take advantage of the energy penetrating deeper inside the receiver, improving the solar radiation absorption and heat transfer enhancement to the circulating fluid, at the time that diminishing the temperature of the surface of the receiver [14, 15]. Another typical application is in actual electronic components, in which big amounts of heat are produced, needing to be dissipated to avoid damage. Microchannel heat sinks, using a porous medium to increase the heat transfer capability of a coolant in contact with a solid, are used to transfer the generated heat to the outside environment [16]. In this context where fluids are present, the thermal conductivity of the fluid is very much important in packed bed systems, in which the contact thermal resistance between particles is very big. The thermal conductivity of the solid increases in importance for better contacts among particles.

Also finished products in which heat transfer is not related to the passing of a fluid are of interest. Thus, good thermal properties for construction materials, with stringent energy regulations and constituted by highly porous building blocks with high resistance to heat transfer, are on times required [17].

Other times the materials to be studied, and in particular their thermal properties, are of interest in a stage previous to their final configuration. Thus, sintering plants use iron ore fines and metallurgical wastes to produce the charge material for blast furnaces in steel plants. This charge material is obtained from a semi-molten mass that solidifies into porous pieces with the adequate size and strength to feed the blast furnace. The knowledge of the thermal properties of the porous charge is necessary to achieve a good blast furnace process performance, including the flame front propagation or gas–solid heat transfer [18]. Another situation in which thermal properties are of interest in an intermediate situation is metals processing through field assisted sintering techniques (FAST) [19]. These sintering techniques use the pass of an electrical current through a powder aggregate to provoke sintering from the heat released by the Joule effect. The knowledge of the thermal properties of the aggregate is a key factor in the proper design of the process [20].

The modelling required is complex for several reasons. The main difficulty resides in the precise knowledge of the microstructure of these complicated porous systems [6]. At present, Computed Axial Tomography equipment makes it possible to know the three-dimensional distribution of porosity [21, 22], which leads us to suspect that there will be important advances in this line of work. On the other hand, models developed for systems with open porosity do not necessarily have to work for those with isolated porosity [9, 23], making necessary specifics models for different situations and materials [6]. When the models have a wider applicability, in general, depend on parameters that must be empirically determined for each material. The complexity increases when there is a fluid flowing through the matrix.

It is logical, therefore, that at present, numerical simulations have been found to be a solution for these situations with complicated three-dimensional structure of the porous materials. Numerical methods precisely describe the complex structure of the porous material up to a certain resolution, being solved by numerical methods [23–26]. Also, the application of the fractal geometry, recognized in several aspects of the microstructure of the materials, is of great interest for porous materials [6, 27]. This current trend, based on massive computation, is absolutely necessary, because it allows to know, as in no other way, the influence of the microstructural characteristics of the porosity.

However, there is no reason why this new trend cannot coexist with simpler mathematical models, valid especially for the first approximations, and which provide a superior understanding of correlations and critical parameters. A review of those models can be found in [13, 28–34]. The proposition of these simple analytical expressions to model the dependence of the thermal (and electrical) conductivity of sintered materials on their porosity was a research challenge during the 1960s–1980s. During those years, many expressions came to be proposed. The realization of the great influence of pore morphology and pore connectivity set the brakes on that work, and the subject was closed in a false sense, as if it had come to be perfectly understood.

Table 1 lists some attempts (some of them very old) that have in common to provide a simple mathematical relationship of dependence on porosity. The methods of deduction have been very varied, and the expressions were deduced in the electric and thermal context, both being transport phenomena in which the influence of the porosity could be described in a similar way.

As expected, for all these models, the conductivity decreases as the porosity increases (the higher the porosity, the smaller the electrical/thermal flow transfer cross-section and the longer the flow path it must take to bypass the pores). Thus, expressions in Table 1 verify that the relative conductivity tends to 1 when the porosity tends to 0, and the conductivity decreases to 0 by increasing the porosity. The upper boundary of Θ is physically restricted in powdered systems to a value lower than 1, which can be assimilated with the tap porosity [56]; the porosity reached by the powder after moderate vibration. (Although the so-called the apparent porosity [57] is slightly higher, its value is less reproducible.).

For this reason, several of the expressions shown in Table 1 can only be considered valid for powdered systems with very low porosities, near 0. Only the expressions by Odelevskii [39], Grootenhuis et al. [40], Loeb [41], McLachlan [45], Gruzdev et al. [46], Montes et al. [47, 52, 54, 55], Pabst et al. [50], and Solonin et al. [51] satisfy the upper

Table 1 Simple expressions for the (thermal or electrical) relative conductivity (g_R), defined as the effective conductivity (g_E) normalised by the conductivity of the fully dense material (g_0)

Authors	Year	Context	$g_R = g_E/g_0$	$g_R \to 1$?	$g_R \to 0$?
Maxwell [35]	1873	Electrical	$\frac{2(1-\Theta)}{2+\Theta}$	$\Theta \to 0$	$\Theta \to 1$
Fricke [36]	1924	Electrical	$\frac{1-\Theta}{1-a\Theta}$	$\Theta \to 0$	$\Theta \to 1$
Austin [37]	1939	Thermal	$\frac{1-\Theta}{1-\frac{1}{2}\Theta}$	$\Theta \to 0$	$\Theta \to 1$
Archie [38]	1942	Electrical	$(1-\Theta)^a$	$\Theta \to 0$	$\Theta \to 1$
Odelevskii [39]	1951	Thermal and electrical (low porosity)	$1-\frac{3}{2}\Theta$	$\Theta \to 0$	$\Theta \to 2/3$
Grootenhuis et al. [40]	1952	Thermal	$1-2.1\,\Theta$	$\Theta \to 0$	$\Theta \to 1/2.1$
Loeb [41]	1954	Thermal (low porosity)	$1-a\,\Theta$	$\Theta \to 0$	$\Theta \to 1/a$
Aivazov and Domashnev [42]	1968	Thermal	$\frac{1-\Theta}{1+a\Theta^2}$	$\Theta \to 0$	$\Theta \to 1$
Koh & Fortini [28]	1971	Thermal and electrical	$\frac{1-\Theta}{1+10\Theta^2}$	$\Theta \to 0$	$\Theta \to 1$
Meyer [43]	1972	Thermal	$\frac{a(1-\Theta)}{a+\Theta}$	$\Theta \to 0$	$\Theta \to 1$
Skorokhod [44]	1974	Thermal and Electrical	$(1-\Theta)^{\frac{3}{2}}$	$\Theta \to 0$	$\Theta \to 1$
McLachlan [45]	1985	Thermal and electrical	$\left(1-\Theta/\Theta_0\right)^{\frac{3}{2}\Theta_0}$	$\Theta \to 0$	$\Theta \to \Theta_0$
Gruzdev et al. [46]	1989	Thermal	$(1-\Theta)^2\left(1-\Theta/\Theta_0\right)^n$	$\Theta \to 0$	$\Theta \to \Theta_0$
Montes et al. [47]	2003	Thermal and electrical	$\left(1-\Theta/\Theta_{\mathrm{M}}\right)^2$	$\Theta \to 0$	$\Theta \to \Theta_{\mathrm{M}}$
Pabst [48]	2005	Thermal	$1-\frac{3}{2}\Theta+\frac{1}{2}\Theta^2$	$\Theta \to 0$	$\Theta \to 1$
Ticha et al. [49]	2005	Thermal	$\exp\left(\frac{-\frac{3}{2}\Theta}{1-\Theta}\right)$	$\Theta \to 0$	$\Theta \to 1$
Pabst and Gregorová [50]	2006	Thermal	$\left(1-\frac{1}{2}\Theta\right)\left(1-\Theta/\Theta_c\right)$	$\Theta \to 0$	$\Theta \to \Theta_c$
Solonin and Chernyshev [51]	2006	Electrical	$(1-\Theta)^{\frac{3}{2}}\left(1-\left(\Theta/\Theta_0\right)^{\frac{4}{3}}\right)^{\frac{1}{2}}$	$\Theta \to 0$	$\Theta \to \Theta_0$
Montes et al. [52]	2008	Electrical	$\left(1-\Theta/\Theta_{\mathrm{M}}\right)^{1+(1-\Theta_{\mathrm{M}})^{4/5}}$	$\Theta \to 0$	$\Theta \to \Theta_{\mathrm{M}}$
Pabst & Gregorová [53]	2012	Thermal	$\frac{(1-\Theta)^2}{1+\frac{1}{2}\Theta}$	$\Theta \to 0$	$\Theta \to 1$
Montes et al. [54]	2016	Electrical	$\left(1-\Theta/\Theta_{\mathrm{M}}\right)^{\frac{3}{2}}$	$\Theta \to 0$	$\Theta \to \Theta_{\mathrm{M}}$
Montes et al. [55]	2018	Electrical	$\left(1-\Theta/\Theta_{\mathrm{M}}\right)^n$	$\Theta \to 0$	$\Theta \to \Theta_{\mathrm{M}}$

In these expressions, Θ is the porosity, Θ_0 is the initial porosity, Θ_{M} the tap porosity, Θ_c a certain critical value of porosity, and the parameters a and n are constants with different value and meaning in each case

boundary condition and, therefore, are of application in the high porosities range. On the other hand, the expression by Odelevskii [39], Grootenhuis et al. [40] and Loeb [41] are experimentally very well validated in the low porosities range. Therefore, it would be desirable that any considered expression was transformed to these equations in the low porosity limit.

Something to consider regarding all these models is the number of parameters involved in them. According to [23] the conductivity models can be divided into rigid models, those involving only thermal conductivity and porosity, and flexible models, containing extra parameters, in many cases without a clear physical meaning. As can be seen in Table 1, most expressions involve an empirical parameter. This is because the conductivity is closely dependent on the microstructure (including pore shape and size), and the empirical parameter helps to model the microstructural influence. Therefore, a simple mathematical expression based only on the porosity level, such as Maxwell expression without any additional empirical parameter, can hardly describe the effective conductivity for high porosities. Several works on sintered materials with more flexible and more complex resulting equations can be found in the literature [58–65], but these equations will not be considered in this study.

In this work, an almost rigid model is proposed for the thermal conductivity of powder aggregates and porous

sintered compacts. The tap porosity of the powder (Θ_M) is the extra parameter considered in the model for powdered materials. Moreover, as in many other models, the effect of pore-filling air conductivity will be analysed and considered negligible. Not much high temperatures will be considered, and therefore radiation heat transfer is neglected. In addition, the Knudsen effect [66], to account for a decrease in conductivity for nanometric sized pores will neither be considered. The model now developed will be compared with other rigid or almost rigid models available in the literature, among the list gathered in Table 1.

2 A new expression for effective thermal conductivity

In previous works [54, 55], the effective electrical conductivity of a porous metallic sintered compact, σ_E, was experimental and theoretically studied. The proposed equation was a function of the electrical conductivity of the fully dense material, σ_0, and the ratio between the porosity of the sample, Θ, and to the tap porosity of the starting powder, Θ_M, with which the compact was manufactured. This tap porosity represents the maximum value that the powder-mass porosity can take in steady states. (Naturally, this parameter depends on the powder particle size, shape and distribution, therefore gathering the morphogranulometric information.) The proposed equation was:

$$\sigma_E = \sigma_0 \left(1 - \Theta/\Theta_M\right)^{\frac{3}{2}} \tag{1}$$

Equation (1) satisfies the expected boundary conditions for the conductivity, $\sigma_E \to \sigma_0$ as $\Theta \to 0$, and $\sigma_E \to 0$ as $\Theta \to \Theta_M$, when interparticle contacts are points.

Equation (l) is also applicable to non-sintered aggregates of non-oxidised particles, because the metallic phase also exhibits connectivity in that case. On the other hand, the electrical behaviour of oxidised metallic powder particles under compression was also studied in [55]. This is the general situation when modelling metallic powders compaction, because particles are usually covered with a nanometric oxide layer (hydroxides can also be present), which is retired (descaling process caused by friction) during powder compression. The equation there proposed to model this new case was:

$$\sigma_E = \sigma_{res} \left(1 - \Theta/\Theta_M\right)^n \tag{2}$$

where σ_{res} is the conductivity at $\Theta = 0$, with a value some lower than σ_0 because of the mechanical descaling process not being completed, and/or because the descaled oxide layers remain in the material, slightly altering the conductivity value despite representing a very small volume fraction. The exponent n is a fitting parameter describing the descaling rate. With very insulating oxide layers, the conductivity will be very low during the first moments of compaction, and the descaling effect will be very pronounced. With oxide-free powders the exponent n is equal to 3/2, but with the presence of oxide layers it takes higher values. The higher or lower difference between the parameters σ_0 and σ_{res}, and how far the parameter n is from the minimum value of 3/2, is due to the influence of the oxide layers, which in general is important.

Naturally, Eq. (2) satisfies the expected limits. Thus, $\sigma_E \to \sigma_{res}$ as $\Theta \to 0$, and $\sigma_E \to 0$ as $\Theta \to \Theta_M$.

Restricting to situations where the temperature is not too high for the transmission by radiation to be significant compared to the conduction mechanism, it is possible to formulate similar expressions that model the thermal conductivity of the porous material. Translating Eq. (1) and Eq. (2) to the thermal case just requires substituting the electrical parameters for those of the thermal context. Thus, κ_E and κ_0 will be the respective values of the effective thermal conductivity and fully dense material thermal conductivity, and κ_{res} the so-called residual thermal conductivity. However, the important role played by the oxide layers in the electrical case (and which justifies the large difference that can exist between the values of σ_0 and σ_{res}) does not hold in the thermal case.

For instance, in the extreme case of the pair aluminium-alumina (metal-oxide), with a typical thickness of 4.5 nm for the oxide layer [67] and a particle radius of 100 μm, and considering electrical resistivities at a temperature of 20 ºC of $\rho_0 = 2.73 \cdot 10^{-8}$ Ωm [68] for the metal and $\rho_X = 1.0 \cdot 10^{-12}$ Ωm [67] for the oxide, a mean electrical resistivity of $4.5 \cdot 10^7$ Ωm is obtained after a volumetric average, which represents a value 15 orders of magnitude higher than that of the pure metal. The situation is completely different for the thermal case. For the same materials, the thermal resistivities are $1/\kappa_0 = 4.22 \cdot 10^{-3}$ $W^{-1} \cdot m \cdot K$ [69] and $1/\kappa_X = 1$ $W^{-1} \cdot m \cdot K$ [70]; averaging in function of the volume a mean resistivity of $4.26 \cdot 10^{-3}$ $W^{-1} \cdot m \cdot K$ is obtained, which is only a 1% higher than that of the pure metal. This means that the influence of the oxide layer can be neglected in the thermal case, and that the translation of Eq. (1) is therefore enough to describe the thermal problem.

However, the simple translation of Eq. (1) could be completed with the contribution to the thermal conduction of the air mass filling the compact pores. This correction was not considered in the electric model because of the much better electrical than thermal insulating effect of the air. For example, for pure aluminium at 20 ºC, $\sigma_{metal}/\sigma_{air} = 7.1 \cdot 10^{21}$ whereas $\kappa_{metal}/\kappa_{air} = 9.1 \cdot 10^3$ [69], therefore resulting an electrical insulating capability around 10^{18} times higher than the thermal one. Thus, it is necessary to study the effect of the thermal conduction of the air filling the pores, mainly for high porosities,

when the conduction in solid state is lower because of the small area of the interparticle contacts.

Admitting that the air contribution is proportional to the normalised porosity, an additional term ($\kappa_{air}\,\Theta/\Theta_M$) has to be added to the translation of Eq. (1), resulting in

$$\kappa_E = \kappa_0\left(1-\Theta/\Theta_M\right)^{\frac{3}{2}} + \kappa_{air}\Theta/\Theta_M \tag{3}$$

Again, Eq. (3) satisfies the expected boundary conditions: $\kappa_E \to \kappa_0$ as $\Theta \to 0$, and $\kappa_E \to \kappa_{air}$ as $\Theta \to \Theta_M$. However, taking into account that $\kappa_{air} = 0.026$ W·m^{-1}·K^{-1} [69] at 20 ºC, for porosity values close to Θ_M, the second term will be negligible considering the much higher experimental uncertainty in the determination of the thermal conductivity and the high values of metallic thermal conductivity. At higher temperatures, for instance 400 ºC, κ_{air} increases up to a value of 0.052 W·m^{-1}·K^{-1} [69], resulting also a small value in practise. Therefore, the model here proposed to describe the thermal conductivity of both metal powder aggregates and porous compacts is the one expressed by:

$$\kappa_E = \kappa_0\left(1-\Theta/\Theta_M\right)^{\frac{3}{2}} \tag{4}$$

This expression is similar to the equations proposed in the percolation field. This context has been suggested many times for modelling and describing transport properties, as it corresponds to heat transfer.

For low porosities (i.e., when $\Theta \to 0$), Eq. (4) can be approximated by Taylor expansion a:

$$\kappa_E \approx \kappa_0\left(1-\left(\frac{3}{2\Theta_M}\right)\cdot\Theta\right) = \kappa_0(1-a\,\Theta) \tag{5}$$

which describes a linear behaviour, often observed and proposed for sintered materials with low residual porosity, and which agrees with the expressions proposed and validated by Grootenhuis et al. [40], and Loeb [41].

On the other hand, for systems in which the maximum porosity, Θ_M, can take values very close to unity, as in foamed materials [71], Eq. (4) becomes

$$\kappa_E = \kappa_0(1-\Theta)^{\frac{3}{2}} \tag{6}$$

which formally fits into the category represented by Archie equation [37], and coincides exactly with the expression proposed by Skorokhod [44] and, years later, also defended by Bauer [72].

At the low porosity limit, Eq. (6) becomes

$$\kappa_E = \kappa_0\left(1-\tfrac{3}{2}\Theta\right) \tag{7}$$

which coincides with the expression from Odelevskii [39], and using Taylor's development, also with the expression from Maxwell [35].

3 Experimental validation

3.1 Equipment and experimental procedure

The measurement of thermal conductivity in small samples with high thermal conductivity has been very difficult until the advent of laser measurement equipment. This equipment is based on the fact that thermal conductivity (κ) can be expressed as the product $\kappa = \alpha \cdot c_p \cdot \delta$, where α is the so-called *thermal diffusivity* (expressed in m^2/s) of the sample, c_p is its *specific heat capacity* (expressed in J/(kg·K)) and δ is its apparent density (expressed in kg/m^3). Thus, the units of κ result W/(m·K), as can be expected. Therefore, to measure the thermal conductivity of samples, three measurements are required: thermal diffusivity, specific heat capacity and apparent density.

A Laser Flash (LFA 1000/1000 HT, from LINSEIS GmbH, Germany) was used to determine the thermal diffusivity (α) of the compacts. With this technique, the sample surface is irradiated with a programmed energy pulse (laser or xenon flash). This energy pulse results in a homogeneous temperature rise at the sample surface. The resulting temperature rise of the rear surface of the sample is measured by a high-speed IR detector and thermal diffusivity values are computed from the temperature rise versus time data (Fig. 1).

The specific heat capacity was determined by Modulated Differential Scanning Calorimetry, MDSC (Q20-DSC, from TA Instruments, USA). This equipment can measure the specific heat capacity of a material in quasi-isothermal mode, i.e. admitting only the small temperature oscillation associated with modulation, which ensures the best level of measurement reliability. The measurements were carried out at room temperature, using a modulation level of ± 1 °C per 120 s.

On the other hand, the apparent density was determined by dimensional measurement of the cylindrical compacts and weighing. Of all the measurements involved, the seemingly simple measurement of apparent density may be the main source of error. Dimensional measurements must be made with great care.

In order to determine the porosity of the compacts, the absolute density, δ_0, of the starting powders must be known. This was determined by pycnometric technique (using Accupyc II 1340, from Micromeritics GmbH, Germany). The determination of the tap porosity is done according to MPIF Standards [56]. Essentially, the method consists of taking 100 g of powder which is poured into a graduated glass tube

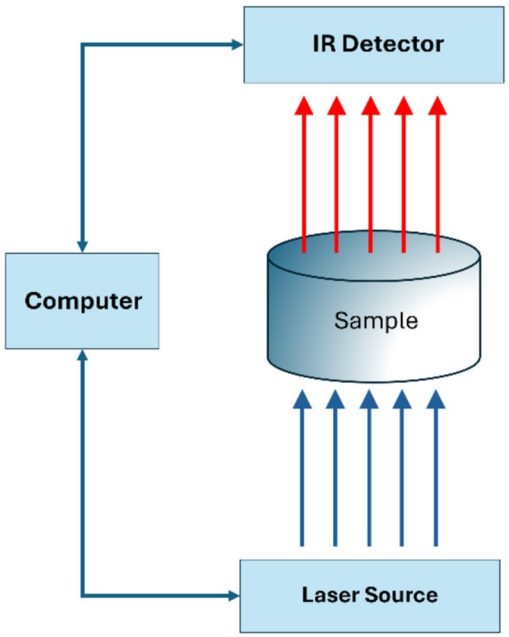

Fig. 1 LFA measuring principle: a laser pulse (in blue) heats the lower base of the sample, and an infrared detector registers the radiation (in red) emitted by the upper base of the sample. A computer calculates the temperature signal as a function of time, from which the thermal diffusivity can be determined

accurate to 0.2 mL. The whole is mechanically tapped, at 150 taps/minute, so that densification can take place without any loosening of surface layers, until the height of the powder column stops decreasing. Then the volume and with it the tap density, δ_T, is determined. In order to calculate the tap porosity, Θ_M, finally we apply $\Theta_M = 1 - \delta_T / \delta_0$.

3.2 Powders

Selected powders with different morphologies, all in commercial grade, have been studied: NC100.24 spongiform iron powder from Höganäs, WPL200 irregular-shaped iron powder from QMP, 4SP400 spherical nickel powder from Novamet, and AS61 irregular-shaped aluminium powder from Eckart-Werke. The very different morphology of the studied powders obtained by scanning electron microscopy (SEM) is shown in Fig. 2.

Table 2 lists, for each type of powder, the absolute density (δ_0), the mean particle radius (r_0), obtained by laser diffraction, and the tap porosity (Θ_M).

The absolute error made in the determination of Θ_M, considering the precision of the instruments employed, can be estimated in ± 0.01; a certainly small value. Nevertheless, during the measuring process, the way and strength of the tapping could account for a non-controlled increase of the

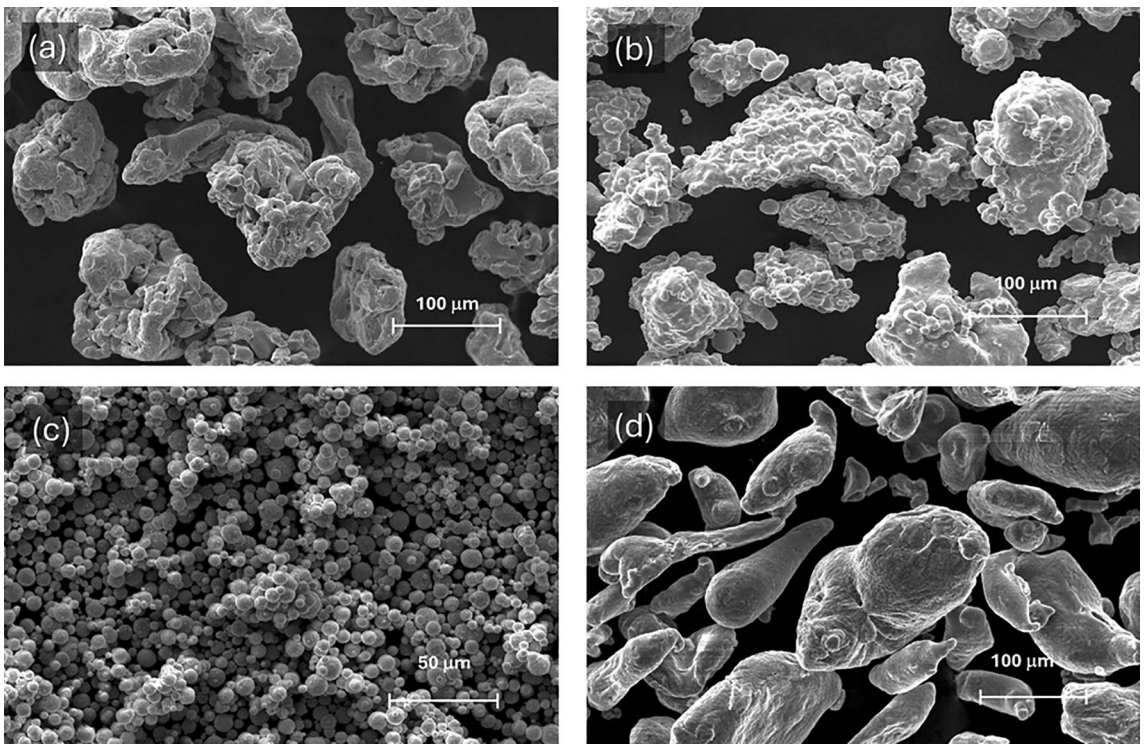

Fig. 2 Micrographs obtained by Scanning Electron Microscopy (SEM) of selected powders: **a** NC100.24 iron, **b** WPL200 iron, **c** 4SP400 nickel and **d** AS61 aluminium

Table 2 Absolute density (δ_0), mean particle radius (r_0) and tap porosity (Θ_M) of studied powders

Powder	δ_0 (g/cm^3)	r_0 (μm)	Θ_M
NC100.24 iron	7.86	55.6	0.65
WPL200 iron	7.87	39.2	0.63
4SP400 nickel	8.91	6.6	0.60
AS61 aluminium	2.70	22.2	0.45

Table 4 Values of the adjustable parameters and the corresponding determination coefficient, obtained after fitting the experimental data to Eq. (4)

Material	κ_0, W/(m·K)	Θ_M	R^2
NC100.24 iron	78.20	0.6058	0.9974
WPL200 iron	78.20	0.6462	0.9920
4SP400 nickel	85.05	0.7614	0.9664
AS61 aluminium	231.71	0.5204	0.9931

experimental uncertainty. Experimental tests, concerning the tapping effect, lead to an uncertainty range of ± 0.05 for Θ_M.

3.3 Samples

For each of the selected powders, cylindrical parts with different porosities were manufactured. The production method was the conventional route of cold compaction and furnace sintering.

Uniaxial cold pressing with a 12 mm inner diameter die was employed for compaction. In each case, the working pressure was determined based on the compressibility curve [73]. The lowest porosity was achieved, in all cases, by applying the maximum available pressure (1400 MPa). The lowest pressure was chosen as the one that allowed to obtain the most porous green compact that was manipulable. This was achieved with compacts with a porosity value such that the Θ/Θ_M ratio is between 0.6 and 0.7, for all powders. The range of porosity studied for each material is detailed in Table 3. The pressing process was followed by a sintering treatment at the temperature indicated in Table 3, for 30 min and under a 1.2 bar argon atmosphere. The temperature was chosen just to increase the green strength, avoiding important changes in the final porosity and thus achieve a cloud of experimental points more or less equispaced on the porosity axis (which has no other rationale than purely aesthetic). Nevertheless, the final porosity after sintering has been again determined by measuring and weighing the compacts, and the obtained value has been the one considered in the later calculations.

The high value chosen for the sintering temperature of aluminium, very close to but lower than its melting temperature, may come as a surprise. This is due to the strength of the oxide layers that surround the aluminium particles, that effectively passivate metal, but also posing an insurmountable barrier to sintering at low temperature (a possible solution would have been to use a reducing atmosphere, H_2, for example).

4 Results and discussion

According to the experimental procedure described in Sect. 3.1, first, the apparent densities of each compact were determined. Secondly, the specific heat capacity (at room temperature) of a sample of each type of material was determined (it does not matter which sample, since this quantity does not depend on porosity and it is practically insensitive to microstructural details, such as grain size, for example). The values obtained were 470 J/(kg·K), 440 J/(kg·K) and 906 J/(kg·K), for iron, nickel and aluminium, respectively. Third and finally, the thermal diffusivities of each compact were determined (at room temperature). With all the information, the value of the thermal conductivities (at room temperature) was calculated.

The thermal conductivity data for all compacts of each material were fitted by least squares to Eq. (4). In this process, both κ_0 and Θ_M were considered as fitting parameters, although both were subject to constraints. On the one hand, Θ_M had to be less than 1 and greater than the porosity of the most porous compact. On the other hand, since the selected materials are only commercially pure, the value of κ_0 should be less than or equal to the thermal conductivity value of the fully dense pure material found in the literature [68] (78.2 W/(m·K) for iron, 88.5 W/(m·K) for nickel and 238 W/(m·K) for aluminium).

Table 3 Porosity range, pressure range, sintering temperature and time for the selected powders

Powder	Porosity range	Pressure range, MPa	Sintering temperature, ºC	Time, min
NC100.24 iron	0.03–0.44	1400–110	1150	30
WPL200 iron	0.02–0.43	1400–90	1150	30
4SP400 nickel	0.06–0.37	1400–330	800	30
AS61 aluminium	0.01–0.32	1400–40	650	30

The values of the adjustable parameters resulting from the fittings are shown in Table 4, together with the coefficient of determination (R^2) that accounts for the goodness of fit in each case.

Figure 3 shows the experimental thermal conductivities for each material versus porosity. Next to the experimental points, the theoretical curve, Eq. (4), resulting from the least squares fitting is also shown.

In general terms, the proposed model given by Eq. (4) causes a good fitting in all the cases, with coefficients of determination higher than 0.99 in three cases, and near 0.97 in one case (corresponding to nickel powder).

The values obtained for κ_0, in accordance with the constraints imposed on the fit, are equal to or slightly lower than the values reported in the literature for the fully dense pure material. The largest difference is found in the case of nickel powder, for which the κ_0 value obtained is 2.6% lower than the value found in literature. This is, however, a perfectly acceptable value.

Concerning the Θ_M parameter, the values obtained for the two iron powders and the aluminium powder fall within the uncertainty interval (± 0.05) of the experimentally determined Θ_M values for these powders. However, in the case of the nickel powder, the value given by the fit is above the

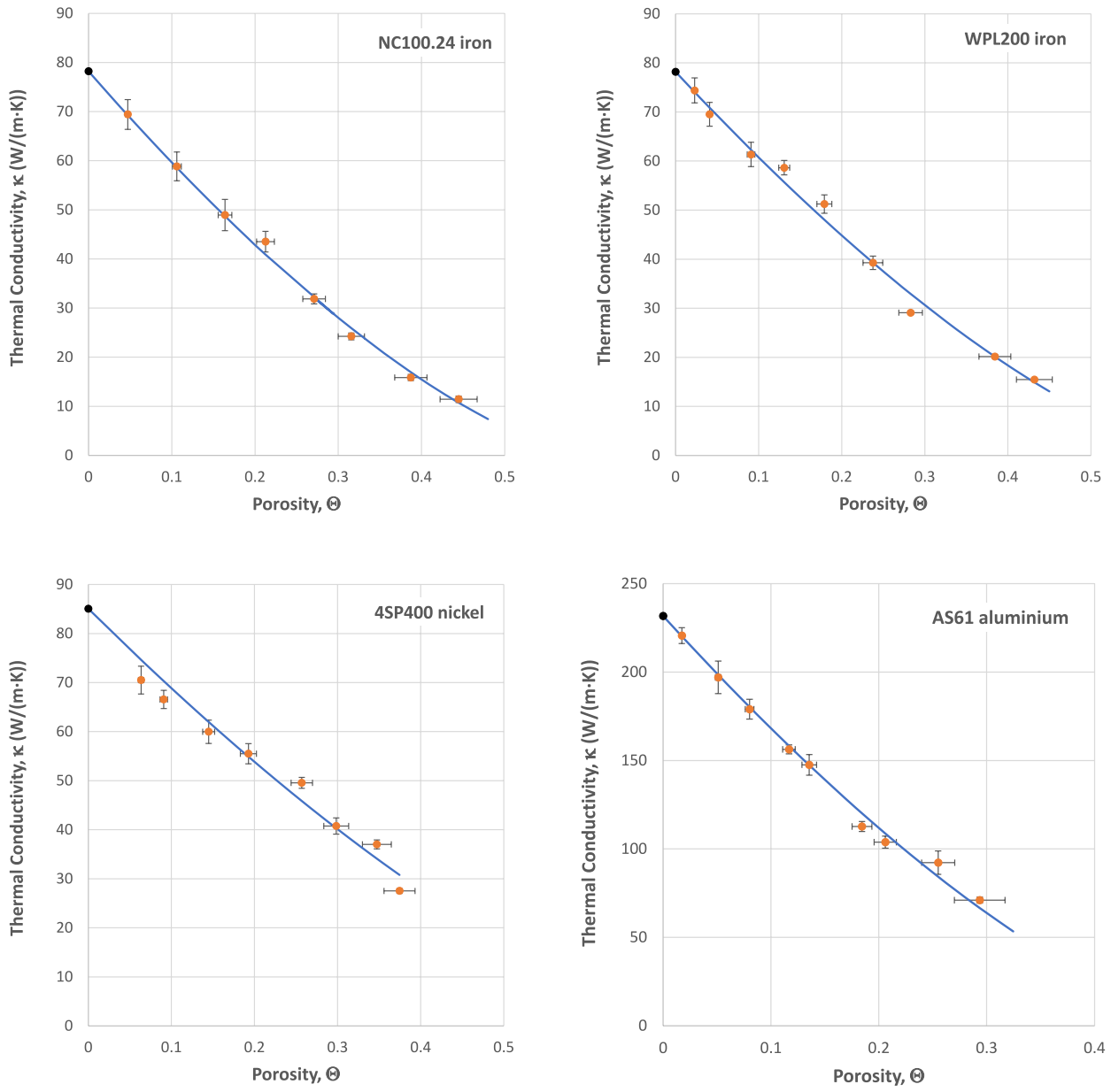

Fig. 3 Variation of the experimental thermal conductivity as a function of porosity and theoretical curve, Eq. (4), obtained by least squares adjustment, for the different materials studied

measured value, considering its upper uncertainty interval. It also happens that this powder is the one that gives the worst fit, according to the value of R^2. An analysis of the characteristics of this powder may lead us to the conclusion that it could be the spherical geometry of the initial powder that is responsible for this greater disagreement. Precisely, this powder morphology is not particularly desirable in Powder Metallurgy, except for very specific applications, especially aimed at favouring the high open porosity of compacts, such as self-lubricating bushings [74]. On the other hand, the SEM images in Fig. 3 reveal that the mean particle size of the nickel powder is clearly smaller than the rest and exhibit little size dispersion. In addition, the particles are aggregated, forming clusters. All these factors, absent in the other powders, could be additional reasons for the larger discrepancy.

Figure 4 shows the experimental data of all the materials in the same graph. For this purpose, the relative thermal conductivity (calculated by normalising by the value of the fully dense material conductivity resultant of the fit) is plotted against the relative porosity (calculated by normalising by the value of the tap porosity obtained in the fit). The collective point cloud has been fitted by least squares to Eq. (4) expressed with relative variables, and the coefficient of determination of the collective fit obtained was $R^2 = 0.9917$. Again, a very acceptable value.

On the other hand, Table 5 shows the results of the least squares fits using various models selected from Table 1 and the experimental data measured in this work. To facilitate the comparison job, the values obtained in the fits with the model proposed here have also been included. The other selected models have been: the Linear law [41], the Archie model [38], the Percolation law [55], the Gruzdev et al. model [46], the Pabst and Gregorová model [50], the Solonin and Chernyshev model [51] and the Aivazov and Domashnev model [42]. Models with 2 and 3 adjustable parameters (some of them subject to the aforementioned constraints) have therefore been included. It would be expected that the goodness of fit would be greater for models with more degrees of freedom, that is, with a greater number of adjustable parameters.

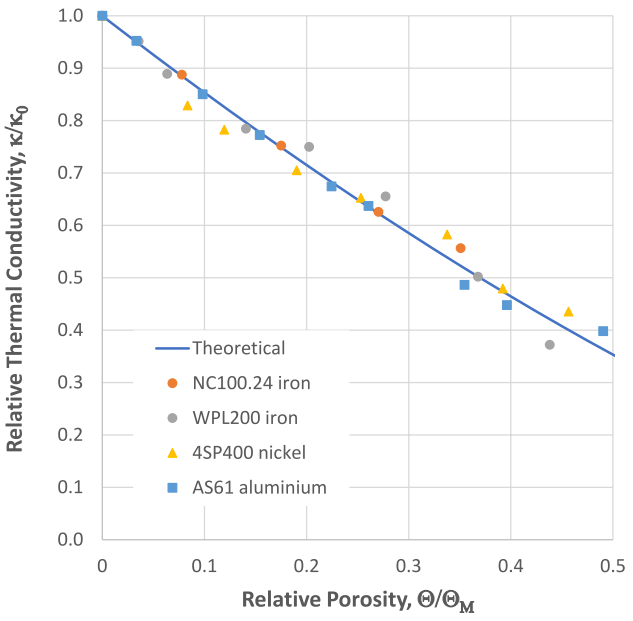

Fig. 4 Experimental data of thermal conductivity for all materials and theoretical curve, from normalised Eq. (4), obtained by least squares fitting

For the NC100.24 iron powder, the model that provides the best fitting among those selected is the Percolation law, with 3 adjustable parameters; 2 subject to constraints (κ_0 and Θ_M) and another one (n) completely free. However, the fitting goodness achieved differs very little from that achieved by the model proposed in this paper, which has only 2 degrees of freedom and with constraints (in κ_0 and Θ_M). The resulting n value in the Percolation law is about 1.4, close to the value of 1.5 set by the model proposed here. On the other hand, the model of Aivazov and Domashnev, with 2 adjustable parameters, provides an also good agreement, only slightly lower than the commented models. For that model, the value of the adjustable parameter a turns out to be 11.08, close to the value of 10 set by Koh and Fortini [28]. Contrary to expectations, it is not the linear law that provides the worst agreement, but the Archie model; both with 2 adjustable parameters.

For the WPL200 iron powder, both the Percolation law and the model proposed here achieve the same degree of agreement. Again, the value of n turns out to be about 1.4, again close to 1.5. An only slightly lower agreement is achieved by the model of Aivazov and Domashnev, with 2 adjustable parameters, and for which the free parameter a now turns out to be worth about 9; close again to the value of 10, set by Koh and Fortini [26]. Also in this case, the linear law provides better agreement than Archie model.

For the 4SP400 nickel powder, all the selected models achieve lower agreements than the rest of the powders. Archie model, Percolation law and the model of Gruzdev et al. achieve the highest R^2 values. However, the values of Θ_M and Θ_0 resulting from the fits are equal to unity, which is not a value consistent with the meaning attributed to them by the respective models, in the context of powdered materials. The model proposed here achieves only slightly lower agreement and a value for Θ_M that is also too high, but less than unity, thus more consistent. The Archie model improves its concordance compared to the other models.

For the AS61 aluminium powder the best agreement is provided, again, by the triad Archie model, Percolation law and the model of Gruzdev et al. As in the case of nickel powder, the resulting values of Θ_M and Θ_0 are

Table 5 Results of fits with selected models proposed by other authors

NC100.24 iron					
Model	κ_0	a	$\Theta_M, \Theta_c, \Theta_0$	n	R^2
This paper	78.2000		0.6058		0.9974
Linear law [41]	75.8678	2.0331			0.9909
Archie model [38]	78.2000			2.8696	0.9881
Percolation law [55]	78.2000		0.5812	1.4074	0.9976
Gruzdev et al. model [46]	78.2000		0.4741	0.2982	0.9956
Pabst and Gregorová model [50]	77.9928		0.5265		0.9969
Solonin and Chernyshev model [51]	75.6886		0.4717		0.9919
Aivazov and Domashnev model [42]	76.3909	11.0880			0.9933
WPL200 iron					
Model	κ_0	a	$\Theta_M, \Theta_c, \Theta_0$	n	R^2
This paper	78.2000		0.6462		0.9920
Linear law [41]	76.5254	1.9435			0.9880
Archie model [38]	78.2000			2.6109	0.9860
Percolation law [55]	78.1885		0.6163	1.3991	0.9922
Gruzdev et al. model [46]	78.2000		0.4663	0.2033	0.9906
Pabst and Gregorová model [50]	78.1200		0.5621		0.9918
Solonin and Chernyshev model [51]	76.7978		0.4974		0.9908
Aivazov and Domashnev model [42]	76.0623	9.0606			0.9920
4SP400 nickel					
Model	κ_0	a	$\Theta_M, \Theta_c, \Theta_0$	n	R^2
This paper	85.0538		0.7614		0.9664
Linear law [41]	83.6171		1.7204		0.9616
Archie model [38]	85.9583			2.1454	0.9682
Percolation law [55]	85.9583		1.0000	2.1454	0.9682
Gruzdev et al. model [46]	85.9583		1.0000	0.1454	0.9682
Pabst and Gregorová model [50]	85.0562		0.6752		0.9664
Solonin and Chernyshev model [51]	85.0562		0.6752		0.9625
Aivazov and Domashnev model [42]	81.5883	4.7409			0.9616
AS61 aluminium					
Model	κ_0	a	$\Theta_M, \Theta_c, \Theta_0$	n	R^2
This paper	231.7065		0.5204		0.9931
Linear law [41]	226.9954		2.4752		0.9832
Archie model [38]	236.2107			3.4067	0.9966
Percolation law [55]	236.1354		0.9790	3.3247	0.9966
Gruzdev et al. model [46]	236.1389		0.9529	1.3308	0.9966
Pabst and Gregorová model [50]	230.2443		0.4397		0.9907
Solonin and Chernyshev model [51]	223.0450		0.3551		0.9768
Aivazov and Domashnev model [42]	223.7947	16.2477			0.9832

very close to unity and, therefore, they are not acceptable according to the physical meaning that the respective models attribute to these parameters. The model proposed in this work provides a somewhat lower agreement (the best of the rest of the models, however) with a physically reasonable value for Θ_M. The linear law and the Aivazov and Domashnev model provide very poor fits.

Thus, the models proposed by other authors that we have analysed also offer reasonable agreements with the experimental data obtained in this work. The degree

of agreement sometimes differs in the fourth decimal place of R^2. However, the values obtained from the fits are not always consistent with the physical meaning that the model attributes to the parameter. Nor does having a greater number of adjustable parameters (especially 3 versus 2) guarantee better agreement. Thus, the proposed model is not only mathematically simple, but despite having only two adjustable parameters, it provides one of the best agreements, while preserving the expected ranges of values for each parameter.

5 Conclusions

A new equation for calculating the effective thermal conductivity of sintered powder materials has been proposed. This equation is obtained through the simplification of a more complex model developed to model the effective electrical conductivity. In the proposed model, only two parameters have been considered: κ_0, the thermal conductivity of the fully dense material, and Θ_M, the tap porosity of the starting powder.

A priori, the proposed model is applicable to sintered compacts of metallic and ceramic powders, but, in this paper, it has only been validated with metal compacts. The fitting between experimental and theoretical values is quite good, obtaining reasonable Θ_M and κ_0 values.

The fit of the experimental data with the models of other authors allows to conclude that those models containing more than two adjustable parameters do not always provide better agreements. In particular, the proposed model is better than the other two-parameter models analysed, since it provides good agreements and yields values for the different adjustable parameters that are within the expected range, according to the meaning attributed to the model.

Author contributions Conceptualization and writing—original draft: J.M. Montes and F.G. Cuevas; investigation: J. Cintas; investigation and validation: F. Ternero; writing—review & editing: all authors.

Funding Funding for open access publishing: Universidad de Sevilla/CBUA. The authors are grateful for the financial support from the Ministerio de Ciencia e Innovación and Agencia Estatal de Investigación (Spain) and Cofunded by the European Union through the research project PID2021-123750OB-I00.

Data availability The datasets generated during the current study are available from the corresponding author on reasonable request.

Declarations

Conflict of interest The authors declare that there is no conflict of interest.

References

1. B. Zhao, A.K. Gain, W. Ding, L. Zhang, X. Li, Y. Fu, A review on metallic porous materials: pore formation, mechanical properties, and their applications. Int. J. Adv. Manuf. Technol. **95**(5–8), 2641–2659 (2018)
2. F.G. Cuevas, J.M. Montes, J. Cintas, P. Urban, Electrical conductivity and porosity relationship in metal foams. J. Porous Mater. **16**, 675–681 (2009)
3. M. Stucki, M. Loepfe, W.J. Stark, Porous polymer membranes by hard templating—a review. Adv. Eng. Mater. **20**, 1700611 (2018)
4. S. Fu, J. Yao, Z. Yang, H. Sun, W. Liu, Silane-based hypercross-linked porous polymers and their applications in gas storage and water treatment. J. Mater. Sci. **53**(14), 10469–10478 (2018)
5. E.C. Hammel, O.L.-R. Ighodaro, O.I. Okoli, Processing and properties of advanced porous ceramics: an application based review. Ceram. Int. **40**(10), 15351–15370 (2014)
6. G. Pia, L. Casnedi, U. Sanna, Porosity and pore size distribution influence on thermal conductivity of yttria-stabilized zirconia: experimental findings and model predictions. Ceram. Int. **42**(5), 5802–5809 (2016)
7. P. Harriott, Thermal conductivity of catalyst pellets and other porous particles part I: review of models and published results. Chem. Eng. J. **10**, 65–71 (1975)
8. E.E. Gonzo, Estimating correlations for the effective thermal conductivity of granular materials. Chem. Eng. J. **90**, 299–302 (2002)
9. J.K. Carson, S.J. Lovatt, D.J. Tanner, A.C. Cleland, Thermal conductivity bounds for isotropic, porous materials. Int. J. Heat Mass Transfer **48**(11), 2150–2158 (2005)
10. W. Pabst, T. Uhlířová, E. Gregorová, A. Wiegmann, Young's modulus and thermal conductivity of closed-cell, open-cell and inverse ceramic foams—model-based predictions, cross-property predictions and numerical calculations. J. Eur. Ceram. Soc. **38**(6), 2570–2578 (2018)
11. R.J. Cai, S.W. Tang, Z. He, The modeling of electrical property in porous media based on fractal leaf vein network. Int. J. Eng. Sci. **123**, 1339–1351 (2018)
12. K. Rumpf, P. Granitzer, H. Michor, Porous silicon nanocomposites with combined hard and soft magnetic properties. Nanoscale Res. Lett. **11**, 398 (2016)
13. B. Sundén, J. Yuan, Evaluation of models of the effective thermal conductivity of porous materials relevant to fuel cell electrodes. Int. J. Comp. Meth. Exp. Meas. **1**(4), 440–455 (2013)
14. M.E. Nimvari, N.F. Jouybari, Q. Esmaili, A new approach to mitigate intense temperature gradients in ceramic foam solar receivers. Renew. Energy **122**, 206–215 (2018)
15. S. Du, Y.-L. He, W.-W. Yang, Z.-B. Liu, Optimization method for the porous volumetric solar receiver coupling genetic

algorithm and heat transfer analysis. Int. J. Heat Mass Transf. **122**, 383–390 (2018)
16. A. Ghahremannezhad, K. Vafai, Thermal and hydraulic performance enhancement of microchannel heat sinks utilizing porous substrates. Int. J. Heat Mass Transf. **122**, 1313–1326 (2018)
17. W. Van De Walle, H. Janssen, A thermal conductivity prediction model for porous building blocks. Bauphysik **38**(6), 340–347 (2016)
18. H. Zhou, M. Zhou, M. Cheng, X. Guo, Y. Li, P. Ma, K. Cen, High resolution X-ray microtomography for the characterization of pore structure and effective thermal conductivity of iron ore sinter. Appl. Therm. Eng. **127**, 508–516 (2017)
19. S. Grasso, Y. Sakka, G. Maizza, Electric current activated/assisted sintering (ECAS): a review of patents 1906–2008. Sci. Technol. Adv. Mater. **10**(5), 1–24 (2009)
20. J.M. Montes, F.G. Cuevas, J. Cintas, S. Muñoz, Thermal conductivity of powder aggregates and porous compacts. Metall. Mater. Trans. A **43**(12), 4532–4538 (2012)
21. Q. Sun, Y. Xia, J. Klinger, R. Seifert, J. Kane, V. Thompson, Q. Chen, X-Ray computed tomography-based porosity analysis: algorithms and application for porous woody biomass. Powder Technol. **388**, 496–504 (2021). https://doi.org/10.1016/j.powtec.2021.05.006
22. S. Nosewicz, G. Jurczak, T. Wejrzanowski, S.H. Ibrahim, A. Grabias, W. Węglewski, K. Kaszyca, J. Rojek, M. Chmielewski, Thermal conductivity analysis of porous NiAl materials manufactured by spark plasma sintering: experimental studies and modelling. Int. J. Heat Mass Transfer **194**, 123070 (2022). https://doi.org/10.1016/j.ijheatmasstransfer.2022.123070
23. J.K. Carson, S.J. Lovatt, D.J. Tanner, A.C. Cleland, An analysis of the influence of material structure on the effective thermal conductivity of theoretical porous materials using finite element simulations. Int. J. Refrig. **26**(8), 873–880 (2003)
24. S. Grandjean, J. Absi, D.S. Smith, Numerical Calculations of the Thermal Conductivity of Porous ceramics based on micrographs. J. Eur. Ceram. Soc. **26**, 2669–2676 (2006)
25. W. Pabst, T. Uhlířová, E. Gregorová, A. Wiegmann, Relative Young's modulus and thermal conductivity of isotropic porous ceramics with randomly oriented spheroidal pores—model-based relations, cross-property predictions and numerical calculations. J. Eur. Ceram. Soc. **38**, 4026–4034 (2018)
26. Y.-H. Dong, C.-A. Wang, L.-F. Hu, J. Zhou, Numerical calculations of effective thermal conductivity of porous ceramics by image-based finite element method. Front. Mater. Sci. **6**(1), 79–86 (2012)
27. S.-F. Wang, T. Wu, A new fractal model for the effective thermal conductivity of porous media. J. Eng. Thermophys. **37**(12), 2626–2630 (2016)
28. J.C.Y. Koh, A. Fortini, Thermal conductivity and electrical resistivity of porous materials, NASA Report No. NAS3-12012, CR-120854, USA, (1971)
29. R.I. Vachon, A.G. Prakouras, R. Crane, M.S. Khader, Thermal conductivity of heterogeneous mixtures and lunar soils, final report NAS8–26579. Auburn University, Department Mechachanical Engineering Thermoscience Group, USA, (1973)
30. E. Tsotsas, H. Martin, Thermal conductivity of packed beds: a review. Chem. Eng. Process. **22**(1), 19–37 (1987)
31. P. Collishaw, J. Evans, An assessment of expressions for the apparent thermal conductivity of cellular materials. J. Mater. Sci. **29**(9), 2261–2273 (1994)
32. L. Gong, Y. Wang, X. Cheng, R. Zhang, H. Zhang, A novel effective medium theory for modelling the thermal conductivity of porous materials. Int. J. Heat Mass Transfer **68**, 295–298 (2014)
33. K. Pietrak, T.S. Wisniewski, A review of models for effective thermal conductivity of composite materials. J. Power Technol. **95**(1), 14–24 (2015)
34. F. Ternero, L.G. Rosa, P. Urban, J.M. Montes, F.G. Cuevas, Influence of the total porosity on the properties of sintered materials—a review. Metals **11**, 730 (2021). https://doi.org/10.3390/met11050730
35. J.C. Maxwell, *A treatise on electricity and magnetism* (Clarendon Press, Oxford, 1873)
36. H. Fricke, A mathematical treatment of the electric conductivity and capacity of disperse systems I. the electric conductivity of a suspension of homogeneous spheroids. J. Physical Rev. **24**, 575–587 (1924)
37. J.B. Austin, Factors influencing the thermal conductivity of nonmetallic materials. In: ASTM symposium on thermal insulating materials, Philadelphia, 1939, 3-67
38. G.E. Archie, The electrical resistivity log as an aid in determining some reservoir characteristics. Pet. Trans. AIME **146**, 54–62 (1942)
39. V.I. Odelevskii, Calculation of general conductivity of heterogeneous systems II. Random mixtures of nonelongated particles. Zh. Tekh. Fiz. **21**(6), 678–685 (1951)
40. P. Grootenhuis, R.W. Powell, R.P. Tye, Thermal and electrical conductivity of porous metal made by powder metallurgy methods. Proc. Phys. Soc. B **65**, 502–511 (1952)
41. A.L. Loeb, Thermal conductivity: VIII, a theory of thermal conductivity of porous materials. J. Am. Ceram. Soc. **37**(2), 96–99 (1954)
42. M.I. Aivazov, I.A. Domashnev, Influence of porosity on the conductivity of hot-pressed titanium nitride specimens. Soviet Powder Metallurgy and Metal Ceramics **7**(9), 708–710 (1968)
43. R. Meyer, Measurement of electrical resistivity to characterize a sintered product. Powder Metall. Int. **4**(2), 63–67 (1972)
44. V.V. Skorokhod, The rheological principles of sintering theory, Nauk. Dumka, Kiev, 1972 (in Russian).
45. D.S. McLachlan, Equation for the conductivity of metal–insulator mixtures. j. Phys. C Solid State Phys. **18**, 1891–1897 (1985)
46. V.A. Gruzdev, Yu.P. Zarichnyak, Yu.A. Kovalenko, Effect of pressing process parameters on the thermal conductivity of cold-pressed porous powder composites. Soviet Powder Metall. Metal Ceram. **28**(3), 164–168 (1989)
47. J.M. Montes, J.A. Rodríguez, E.J. Herrera, Thermal and electrical conductivities of sintered powder compacts. Powder Metall. **46**(3), 251–256 (2003)
48. W. Pabst, Simple second-order expression: for the porosity dependence of thermal conductivity. J. Mater. Sci. **40**(9–10), 2667–2669 (2005)
49. G. Ticha, W. Pabst, D. Smith, Predictive model for the thermal conductivity of porous materials with matrix-inclusion type microstructure. J. Mater. Sci. **40**(18), 5045–5047 (2005)
50. W. Pabst, E. Gregorová, A new percolation-threshold relation for the porosity dependence of thermal conductivity. Ceram. Int. **32**, 89–91 (2006)
51. S.M. Solonin, L.I. Chernyshev, a percolation approach to conductivity dependence on porosity. Powder Metall. Met. Ceram. **45**(5–6), 226–229 (2006)
52. J.M. Montes, F.G. Cuevas, J. Cintas, Porosity effect on the electrical conductivity of sintered powder compacts. Appl. Phys. A **92**, 375–380 (2008)
53. W. Pabst, E. Gregorová, The sigmoidal average-a powerful tool for predicting the thermal conductivity of composite ceramics. In: 6th European thermal sciences conference, 4–7 September 2012, France

54. J.M. Montes, F.G. Cuevas, J. Cintas, J.M. Gallardo, Electrical conductivity of metal powder aggregates and sintered compacts. J. Mater. Sci. **51**, 822–835 (2016)
55. J.M. Montes, F.G. Cuevas, J. Cintas, F. Ternero, E.S. Caballero, Electrical resistivity of powdered porous compacts, in *Electrical and electronic properties of materials*. ed. by Md. KawsarAlam (InTechOpen, London, 2018), pp.1–18
56. MPIF Standard 46, Determination of tap density of metal powders. In: Standard test methods for metal powders and powder metallurgy products. MPIF, Metal Powder Industries Federation, Princeton (2016)
57. MPIF Standard 4, *Determination of apparent density of free-flowing metal powders using the hall apparatus* (MPIF, Metal Powder Industries Federation, Princeton, 2016)
58. J.P.M. Florez, M.B.H. Mantelli, G.G.V. Nuernberg, F.H. Milanez, Powder geometry based models for sintered media porosity and effective thermal conductivity. J. Thermophys. Heat Transfer **28**(3), 507–517 (2014)
59. A.S. Rogachev, K.V. Kuskov, D.O. Moskovskikh, A.A. Usenko, A.O. Orlov, N.F. Shkodich, M.I. Alymov, A.S. Mukasyan, Effect of mechanical activation on thermal and electrical conductivity of sintered Cu, Cr, and Cu/Cr composite powders. Doklady Phys. **61**(6), 257–260 (2016)
60. N. Atabaki, B.R. Baliga, Effective thermal conductivity of water-saturated sintered powder-metal plates. Heat Mass Transfer **44**(1), 85–99 (2007)
61. X.-L. Ouyang, R.-N. Xu, L. Zhang, B. Zhou, P.-X. Jiang, Prediction of effective thermal conductivity of sintered porous media with the discrete element method. In: Proceedings of the 15th international heat transfer conference, IHTC 2014, Kyoto, Japan, 10–15 August 2014
62. J. Ordonez-Miranda, M. Hermens, I. Nikitin, V.G. Kouznetsova, S. Volz, Modeling of the effective thermal conductivity of sintered porous pastes. In: 20th international workshop on thermal investigations of ICs and systems (THERMINIC), 2014
63. J.P.M. Florez, M.B.H. Mantelli, G.G.V. Nuernberg, Effective thermal conductivity of sintered porous media: model and experimental validation. Int. J. Heat Mass Transf. **66**, 868–878 (2013)
64. S. Mo, P. Hu, J. Cao, Z. Chen, H. Fan, F. Yu, Effective thermal conductivity of moist porous sintered nickel material. Int. J. Thermophys. **27**(1), 304–313 (2006)
65. M. Kurashige, M. Mishima, K. Imai, Simulated effective thermal conductivity of sintered, randomly packed spheres and statistical structures of packings. J. Therm. Stresses **22**(7), 713–733 (1999)
66. P.P. Mukherjee, V.P. Schulz, J. Becker, E. Glatt, A. Wiegmann, Microstructure reconstruction and transport simulation in polymer electrolyte membrane fuel cells, in *Woodhead publishing series in energy, polymer electrolyte membrane and direct methanol fuel cell technology*, vol. 1, ed. by C. Hartnig, C. Roth (Woodhead Publishing, Cambridge, 2012), pp.219–255
67. W.T. Li, D.R. McKenzie, W.D. McFall, Q.C.H. Zhang, W. Wiszniewski, Breakdown mechanism of Al_2O_3 based metal-to-metal antifuses. Solid State Electron. **44**, 1557–1562 (2000)
68. E.A. Brandes (ed.), *Smithells metals referente book*, 6th edn. (Butterworths, UK, 1983)
69. CRC Handbook Of Chemistry And Physics, 80th edition, CRC Press, 1999–2000, New York.
70. S.M. Lee, D.G. Cahill, Thermal conductivity of sputtered oxide films. Phys. Rev. B **52**(1), 253–257 (1995)
71. F.G. Cuevas, J.M. Montes, J. Cintas, P. Urban, Electrical conductivity and porosity relationship in metal foams. J. Porous Mater. **16**(6), 675–681 (2009)
72. T.H. Bauer, A general analytical approach toward the thermal conductivity of porous media. Int. J. Heat Mass Transfer **36**(17), 4181–4191 (1993)
73. Standard test methods for metal powders and powder metallurgy products. Method for determination of compressibility of metal powders. Princeton (NJ): Metal Powder Industries Federation (MPIF); 2002. Standard 45.
74. R.M. German, *Sintering theory and practice*, 1st edn. (John Wiley & Sons, New York, 1996)